PHYSICAL REVIEW B VOLUME 34, NUMBER 4 15 AUGUST 1986

Modeling of nonequilibrium melting and solidification in laser-irradiated materials

R. F. Wood
Solid State Division, Oak Ridge National Laboratory, Oak Ridge, Tennessee 37831

G. A. Geist
Engineering Physics and Mathematics Division, Oak Ridge National Laboratory, Oak Ridge, Tennessee 37831
(Received 24 March 1986)

A computational model has been developed for treating various aspects of the complex melting and solidification behavior observed in pulsed-laser-irradiated materials. An important feature of the modeling is the capability of allowing nonequilibrium melting and solidification to occur at temperatures other than the thermodynamic phase-change temperatures. As a result, interfacial undercooling and overheating can be introduced and various types of nucleation events can be simulated. Calculations for pulsed-laser-irradiated silicon containing amorphous layers have shown a wide variety of behavior, including the formation and propagation of multiple phase fronts and buried molten layers. Although originally developed as a tool for studying problems arising in the field of laser annealing of semiconductors, the approach used in the modeling should be useful in treating many types of systems in which ultrarapid phase change and nucleation phenomena play important roles.

I. INTRODUCTION

In the research described here, we developed the conceptual foundation, and a mathematical model based on it, for the study of heat conduction and phase-change problems associated with the ultrarapid melting and solidification induced by pulsed laser irradiation of semiconductors.[1] LASER8, a computer program implementing the modeling, will be mentioned frequently here but it is described at length elsewhere.[2] The research was stimulated by the inability of commonly available computer programs, e.g., the HEATING series,[3–5] to treat phase-change problems with sufficient generality. Such programs customarily assume that melting and solidification occur at or very near thermodynamic phase-change temperatures and that the introduction of interfacial kinetics into the modeling is unnecessary. The motion of phase interfaces induced by pulsed laser irradiation of materials can be so rapid that this assumption is no longer valid and strong undercooling (and possibly overheating) of the material in various phases must be considered. This capability has been incorporated in our approach by emphasizing the enthalpy rather than the temperature, and by the introduction of the state array through which the state of the material in each small volume element (e.g., a finite-difference cell) is continuously monitored and controlled. The state array also allows the simulation of bulk and interfacial nucleation effects to be included in the modeling. At present, such simulations are handled in a fairly elementary way, but more complex treatments can be incorporated at a later time.

The calculations carried out to date have been restricted to problems that can be approximated by a one-dimensional analysis, i.e., semi-infinite, slab, and spherically symmetric geometries. Conceptually, the modeling is much more general and it is anticipated that this restriction on the present computer program will be removed after accumulating experience with one-dimensional applications.

In the next section, we first describe two classes of experimental observations that illustrate the need for the type of modeling introduced here, we then review briefly classical solidification and nucleation theories, and lastly give an overview of the mathematical approach we found most useful in developing the program. In Sec. III, the finite-difference formulation of the model and our implementation of it are discussed. In Sec. IV, an explanation is given of the manner in which changes of phase and state, overheating and undercooling, and nucleation can be treated in the modeling. This explanation involves a detailed description of state diagrams and state arrays, and examples of how they can be constructed and used in a computer program. Results from the extensive testing of LASER8 are illustrated and discussed in Sec. V, and the paper ends with a few concluding remarks about various aspects of the work.

II. EXPERIMENTAL AND THEORETICAL BACKGROUND

A. Some effects of high-power laser pulses on semiconductors

Pulsed laser processing of materials, especially semiconductors, is a field of condensed-matter physics and materials science that has developed rapidly over the last few years.[1] It has proved to be of considerable interest for both applied and fundamental research for a variety of reasons discussed extensively in the literature.[6] We are most interested in it here because it provides a unique tool for well-controlled studies of physical processes occurring far from thermodynamic equilibrium. To be more specif-

 ©1986 The American Physical Society

ic, irradiation of semiconductors with nanosecond and picosecond pulses from high-powered lasers can result in complex changes of the near-surface regions brought about by ultrarapid melting and solidification. There are two classes of observations in silicon that illustrate complementary aspects of the processes to be modeled here.

The first class demonstrates that when liquid (l) silicon is caused to solidify in a $\langle 100 \rangle$ direction with a phase-front velocity of 15–20 m/sec (by a proper choice of laser pulse), the solid regrows in an amorphous (a) rather than crystalline (c) state.[7–9] There is good evidence that the melting temperature T_a of a-Si is $\sim$150–300 °C lower than T_c,[10] the melting point of c-Si. The formation of a-Si from l-Si would then seem to imply that an undercooling of the liquid of at least $T_c - T_a$ has been achieved without nucleation and growth of the crystalline phase; thus, the inclusion of liquid-phase undercooling is essential in mathematically modeling the ultrarapid solidification involved in this example.

The complementary observations involve the pulsed laser melting of an a-Si layer, formed on or in a c-Si substrate by a variety of techniques, and the subsequent solidification of the l-Si.[11–16] The upper schematic illustration in Fig. 1 represents the initial condition of a sample consisting of a c-Si substrate with an a-Si surface layer formed, for example, by ion implantation. When this a-Si layer is partially melted by a laser pulse, highly undercooled l-Si is formed ($T \simeq T_a$ near the interface between the a- and l-Si). After such a pulse it is observed that two regions of polycrystalline silicon (p-Si) have been formed and the extent of these regions varies with the pulse energy density E_l. For values of E_l just above the threshold for melting of the a-Si, only a fine-grained (FG) p-Si is formed. As E_l is increased, a region of large-grained (LG) p-Si begins to appear in the region nearest the surface, followed in succession by the FG material, the a-Si, and finally the c-Si substrate; this situation is indicated in the lower illustration of Fig. 1. As E_l is increased still further, the LG region increases at the expense of the FG and amorphous regions until both of these disappear altogether. At sufficiently high values of E_l, the LG p-Si is no longer formed and only single-crystal material is observed. The lowest E_l at which this occurs is interpreted as the value required to melt through the a-c interface and produce liquid-phase epitaxy from the c-Si substrate; the c-Si formed in this way is virtually defect free. Further complicating this already complex behavior is the recent observation[17] that large-scale two- and three-dimensional features may be superimposed on the essentially one-dimensional geometry of Fig. 1.

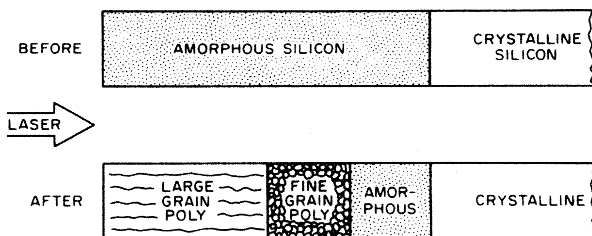

FIG. 1. Illustration of the morphological changes induced by pulsed laser irradiation of an a-Si overlayer on a c-Si substrate.

B. Classical crystal growth theory

The classical phenomenological theory of crystal growth[18–20] expresses the velocity of a liquid-solid interface as the difference between forward and reverse kinetic rate constants, i.e.,

$$v = K^f - K^r . \tag{1}$$

K^f is the rate (in velocity units) at which atoms leave the liquid and join the solid, while K^r is the rate for the reverse process. K^f and K^r are generally considered to represent activated processes and are written as

$$K^f = A^f \exp(-\Delta H^{ls}/kT), \quad K^r = A^r \exp(-\Delta H^{sl}/kT) . \tag{2}$$

ΔH^{ls} and ΔH^{sl} are the activation energies, defined by reference to Fig. 2, and T is the temperature. From Fig. 2 it can be seen that $\Delta H^{ls} - \Delta H^{sl}$ is L_c, the latent heat of crystallization per atom. By simple algebraic manipulation of Eqs. (1) and (2), an expression for the melt-front velocity can be obtained in the form

$$v = K^f(T_i)\{1 - \exp[-(L_c/kT_c)(\Delta T_i/T_i)]\} , \tag{3}$$

in which T_c is the crystallization temperature, T_i is the "interface temperature," and the interfacial undercooling ΔT_i is given by $\Delta T_i = T_c - T_i$. The functional form of Eq. (3), although almost certainly overly simplified, is important because it demonstrates that $\Delta T_i \neq 0$ is necessary for any motion of the interface (undercooling of the liquid for solidification and overheating of the solid for melting) and illustrates how the velocity of the melt front may depend on atomic processes in the interface region. Here we will be concerned primarily with undercooling, but questions concerning overheating for melting are also of considerable interest.

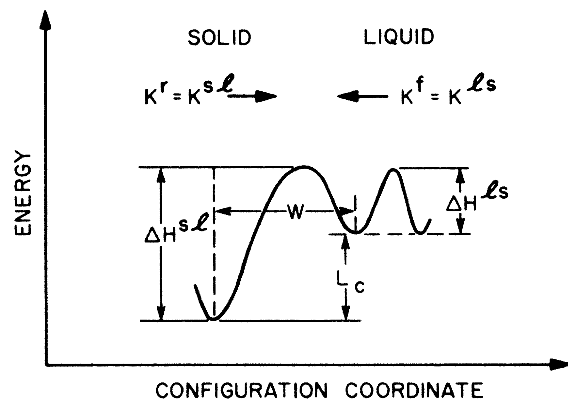

FIG. 2. Kinetic processes at the liquid-solid interface. L_c is the latent heat of crystallization, W is the width of the interfacial region, and the ΔH are activation energies, or enthalpies. K^f is the forward ($l \rightarrow s$) rate constant and K^r is the reverse ($s \rightarrow l$).

The velocity of a planar crystallization front can be obtained from the one-dimensional heat-flux boundary condition at the liquid-solid interface, i.e.,

$$\frac{dQ}{dt} = A\rho L_c \frac{dx}{dt} = K_l[\mathrm{grad}T]_{i,l} - K_s[\mathrm{grad}T]_{i,s} \ . \quad (4)$$

The product $A\,dx$ is the volume of material changing phase in time dt, ρ is the density, K_l and K_s are the thermal conductivities in the liquid and solid, respectively, and the square-bracket notation indicates that the gradients of T in the liquid and solid are to be evaluated at the interface. It is usually assumed in calculating the gradients that the interface is at the thermodynamic phase-change temperature T_c. This assumption, Eq. (4), and the heat-diffusion equation yield the classical Stefan problem.[21–23] We note again that if the interface temperature were actually T_c, ΔT_i in Eq. (3) would be zero and there would be no movement of the phase front. For small values of ΔT_i, the errors made in calculating the gradients as though the interface were at T_c should be very small, and the velocity of the interface given quite accurately by Eq. (4) with $T_i = T_c$. If ΔT_i becomes large, this may no longer be the case [particularly because of the activated rate constant appearing in Eq. (3)] and it will be necessary to introduce interfacial undercooling effects. When the motion of the melt front is controlled by an equation like Eq. (3), it is said to be limited by the interfacial kinetics, otherwise it is said to be heat-flow limited.

C. Phenomenological nucleation theory

Nucleation theory[18,24] deals with the problem of how a new phase begins to form in a material not initially containing that phase. It will be assumed that some type of nucleation event must occur to initiate growth of small nuclei, or seeds, of the new phase, as, for example, in the case illustrated in Fig. 1 in which FG and LG p-Si are formed from undercooled l-Si separated from c-Si by an a-Si layer. Nucleation may occur at free surfaces or interfaces, at impurities or impurity aggregates, or it may in principle occur homogeneously in the bulk of the pure material through statistical fluctuations. In amorphous materials formed by ion implantation, sputtering, or electron beam evaporation, it is possible that minute inclusions of crystalline material are sometimes embedded in the amorphous phase.

Although true homogeneous bulk nucleation probably is rare, an elementary discussion of it will be given here to illustrate the general ideas involved in all phenomenological nucleation theories. A recent paper by Grant and Gunton[25] provides an extensive list of references on the subject and we note that molecular-dynamics treatments are beginning to provide insights into nucleation and interfacial processes on the atomic level.[26]

To be specific, let us assume that a molten material, totally devoid of impurities, is enclosed in a container with which it has no interactions that will nucleate a phase change. As the temperature of the liquid is lowered below the thermodynamic phase-change temperature, the liquid phase becomes metastable relative to the solid phases. At any given undercooling, clusters of atoms may begin to form into solidlike configurations. However, these clusters will generally be unstable because the surface energy of the phase interface is greater than the energy gained by formation of the more stable solid phase. Stated another way, the liquid is constantly undergoing local fluctuations from the liquid to the solid state, but the probability that the fluctuations will result in solid nuclei large enough to be stable and to begin to grow is exceedingly small. As the temperature is lowered still further, the size of a critical nucleus becomes small enough and the fluctuations large enough that stable nuclei can form and grow. The nucleation rate then increases so rapidly over a small temperature range that it is a good approximation to speak of a nucleation temperature.

The foregoing can be formulated quantitatively for spherical nuclei as follows. For a nucleus of radius r the change of free energy associated with the formation of the nucleus is given approximately by

$$\Delta G = 4\pi r^2 \sigma + 4\pi r^3 \Delta G_v / 3 \ , \quad (5)$$

in which σ and ΔG_v are the interfacial and volume free energies, respectively. Setting $d\,\Delta G/dr = 0$ gives

$$r^* = -2\sigma/\Delta G_v, \quad n^* = 4\pi r^{*3} N_v / 3 \ , \quad (6)$$

and

$$\Delta G^* = 16\pi\sigma^3 / 3(\Delta G_v)^2 \ . \quad (7)$$

r^* is radius of the critical nucleus in the undercooled liquid, n^* is the number of atoms in it, and N_v is the number of atoms per unit volume. If the difference in heat capacity between the liquid and crystalline solid can be neglected, ΔG_v can be expressed in terms of the interfacial undercooling as

$$\Delta G_v = -L_c \, \Delta T_i / T_c \ . \quad (8)$$

The interfacial free energy is seldom known accurately, which makes it difficult to estimate ΔG^*. For our purposes, however, it is sufficient to recognize that ΔG^* is the free-energy barrier that must be surmounted for a nuclei to reach critical size and begin to grow. The temperature at which this occurs can be referred to as the nucleation temperature T_n.

The nucleation rate is given in terms of ΔG^* by

$$I = I_0 \exp(-\Delta G^* / kT_i) \ , \quad (9)$$

in which I_0 has the units of $\mathrm{cm}^{-3}\mathrm{s}^{-1}$. The nucleation rate may be a difficult quantity to determine experimentally if it is high because of lack of time resolution in the experiments. Again, however, from the standpoint of our present goal of roughly simulating nucleation processes, it is enough to recognize that a nucleation temperature and rate (or time) can be introduced into the simulations.

It is apparent from the foregoing discussion that nucleation events are likely to be two- and three-dimensional processes and we must be concerned about how they and the subsequent growth of the nuclei can be simulated in a one-dimensional calculation. This will be discussed later after the finite-difference equations have been introduced.

D. Mathematical approach

A variety of methods[27] for treating moving-boundary problems[22,28] was investigated during the course of the development of our approach and the LASER8 computer program.[2] A method was sought that would enable the physical problems discussed above to be studied, and that would serve as a basis for a flexible and efficient finite-difference, or finite-element, program. A method, apparently first developed by Rose,[29,30] that emphasizes the fundamental role of enthalpy in a phase-change process and uses the temperature simply to determine the heat fluxes was finally chosen. This approach has the advantage that the determination of a phase or a state of a small volume of material is based on its enthalpy content rather than its temperature. Thus, a phase change can occur, in principle, at any temperature, with the result that overheating and undercooling can be included in the formalism. A relationship between the extent of overheating or undercooling and the velocity of the phase interface must be specified as a boundary condition (see the discussion in Sec. II B), but this condition need not be restricted to the commonly used requirement that the phase change occur at the equilibrium thermodynamic melting temperature. For the same reason, nucleation effects can be treated because a material can be overheated or undercooled to a prescribed nucleation temperature and held there for a prescribed time before the latent heat of the nucleating phase comes into play. To realize the full flexibility of this method, the various changes of phase and state, and the conditions under which they can occur, can be specified by the state array introduced below.

III. HEAT CONDUCTION AND STATE CHANGE

A. General assumptions

The laser-irradiated sample is modeled as either a slab or a semi-infinite solid extending in the positive x direction and composed of any number of layers, each initially of arbitrary thickness but uniform composition. The laser pulse is assumed (1) to have a cross section large compared to the depth into the sample for which significant temperature changes occur and (2) to be homogeneous in energy across any y-z plane. Experimentally, condition (1) is easily realized in a multitude of cases and, with care, (2) can probably be approximated adequately, although complete homogeneity is basically unattainable and the lack of it may be particularly important around the threshold for melting. As a result of these conditions, the laser annealing process can be treated as a one-dimensional problem, *provided* that any nucleation effects to be included can be usefully simulated within the framework of a one-dimensional approximation.

The optical and thermal properties of the individual layers of the sample may be functions of temperature, phase, and state. For example, with reference to the case illustrated in Fig. 1, it is well known that the materials properties of a-, c-, and l-Si are quite different (see Fig. 4 for the thermal conductivity of a-, c-, and l-Si), but it is also likely that a property such as the thermal conductivity of polycrystalline silicon depends on the grain sizes, shapes, and relative orientations. Provisions for handling these differing properties can be incorporated into a computer program, although it is often difficult to know reliable values of the input data for a complex state.

The left boundary, i.e., the surface at $x=0$, is assumed to be insulated. Calculations have shown that this is a good approximation for laser pulses of nanosecond and picosecond duration because the times involved are too short for convection or radiation losses[5] to be important. Should such losses become important for long-duration pulses, they can easily be included in the modeling. If the sample is semi-infinite, the temperature of the right boundary is assumed to remain constant at its initial value throughout a calculation; calculations for a finite slab may require other boundary conditions.

B. Enthalpy form of the heat-flow equation

It has been customary in most treatments of heat-flow problems to focus attention on the temperature distribution $T(x,t)$ in the sample. In the laser-irradiation case, this leads to the usual partial differential equation for $T(x,t)$ with the expression for the energy in the laser pulse providing a heat source term S.[5] We have not found this a convenient method for dealing with problems in which phase changes can occur at temperatures that may vary during the problem, e.g., when undercooling must be taken into account. Instead, we have employed the above-mentioned method developed by Rose, which is based on an enthalpy formulation of heat flow.[31] It is straightforward to convert the differential equation for $T(x,t)$ into an equation for the enthalpy $h(x,t)$, with the result that after several approximations and simplifications the diffusion equation can be written as

$$\frac{\partial}{\partial t}(\rho h)=\nabla\cdot(K\nabla T)+S \ . \tag{10}$$

In one dimension this becomes

$$\frac{\partial}{\partial t}(\rho h)=\frac{\partial}{\partial x}\left[K\frac{\partial T}{\partial x}\right]+S \ , \tag{11}$$

which is the starting point for the discretization used in constructing the LASER8 computer program.[2] A further simplification is often possible because ρ is very nearly independent of temperature and phase for many materials, e.g., silicon, and hence does not change with time.

We note that in many papers dealing with phase-change problems the authors add to Eq. (11) a term which explicitly displays the time dependence of the latent heat of the phase change, treating the latent heat as a separate source term. This could be done here too, of course, but the finite-difference formulation of the problem and the introduction of the state array make it both unnecessary and undesirable.

C. Source term

The absorption of energy from the laser pulse and its conversion into heat are regarded as providing the only contribution to S in Eq. (11). Even with this restriction,

the heat source term can become very complicated and a detailed discussion of it here would be inappropriate. Instead, we give a simple treatment that is valid for many cases, and then briefly indicate some of the complexities that may arise.

Because the penetration depth of the laser radiation may be comparable to the region over which significant temperature changes occur, it is not accurate to assume that the energy supplied by the laser pulse can be represented simply by a flux term at the surface of the sample. For a constant absorption coefficient α (linear regime), the amount of energy penetrating to a particular depth at time t can be approximated by

$$S(x,t)=[1-R(x,t)]P(t)\alpha e^{-\alpha x}\ , \qquad (12)$$

where $R(x,t)$ is the reflectivity of the sample and $P(t)$ gives the variation in intensity of the laser pulse with time. Reflection of light from a material is not a purely surface phenomena and can therefore depend on both x and t, primarily because of the change in temperature and phase with x and t. For simplicity, we assume here that R is a function only of the temperature and phase of the surface. $P(t)$ is often very nearly a Gaussian for solid-state lasers, but can have complex forms for gas lasers; a typical excimer laser pulse shape is shown in Fig. 3. Although the sharp structure on this pulse need not be duplicated, the overall shape should be reproduced reasonably well. To determine the amount of energy that is deposited in a finite-difference cell, the factor $\alpha\exp(-\alpha x)$ in Eq. (12) can be integrated to yield a simple analytical relation for determining the energy generation rate. The transfer of energy from the carrier system to the lattice occurs on the picosecond time scale,[32] so that for nanosecond laser pulses the energy and heat generation rates are essentially identical.

It may happen that the absorption coefficient α is not constant, and then the simple treatment given here no longer holds. It is not difficult to include temperature- and intensity-dependent (nonlinear) absorption in the modeling, but the values of α for the laser radiation used in the experiments of interest to us to date are so high ($\geq 10^6$ cm^{-1}) that these effects are relatively unimportant. For long-wavelength radiation, such as that from a CO_2 laser, α for a semiconductor can be expected to be a complex function of doping concentration, temperature, radiation-induced free carriers, carrier diffusion, etc.

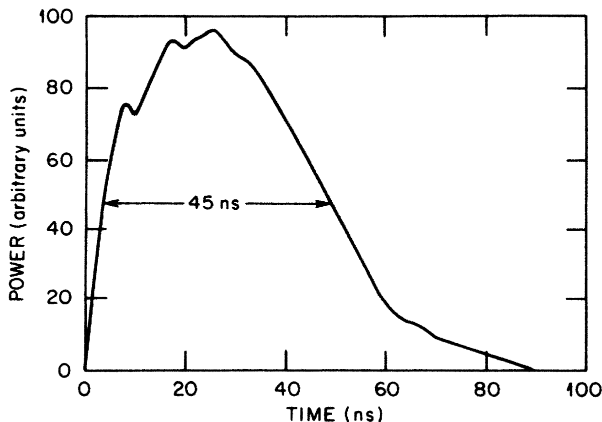

FIG. 3. The time dependence of a typical excimer laser pulse.

D. Discretization

Equation (11) was discretized using the classical forward time difference scheme. This gives an explicit method for updating the enthalpies from time step n to $n+1$. For the ith cell in the bulk of the material the finite-difference equation becomes

$$\rho\frac{h_i^{n+1}-h_i^n}{\Delta t}=\frac{1}{(\Delta x)^2}\left[\frac{K_{i+1}+K_i}{2}(T_{i+1}^n-T_i^n)+\frac{K_i+K_{i-1}}{2}(T_{i-1}^n-T_i^n\right]+S_i^n\ . \qquad (13)$$

It should be noted that the effective thermal conductivity for heat conduction between cells i and $i+1$ is given as an average of the conductivity in the two cells. The question of how to treat the conductivity of a cell that is partially solid and partially liquid is considered in Ref. 2.

Since we have assumed the surface to be insulated, the appropriate boundary conditions on the temperature and energy profiles can be obtained by reflection of these profiles in the plane of the surface. The second-order discretization scheme can then be preserved if the surface cell is half as wide as a bulk cell and the method of images is used. Thus the equation for the surface node becomes

$$\rho\frac{h_1^{n+1}-h_1^n}{\Delta t}=2\frac{K_1+K_2}{(\Delta x)^2}(T_2^n-T_1^n)+S_1^n\ . \qquad (14)$$

There were two main reasons why a more complex discretization scheme (for example, the Crank-Nicholson scheme) was not used. First, the intensity of the source term is often so large and changing so rapidly that small time steps are generally required to describe it. The intensity of the laser pulse may also cause the melt front to move at very high velocities. The advantage of using higher-order schemes is that they typically allow much larger time steps at the cost of computational effort. Since in most of the cases of interest here the time step must be small to track the front accurately and model the laser pulse satisfactorily, this advantage is lost. Second, state arrays are set up on the assumption that only one change of phase can occur in a time step. This is a reasonable assumption only if the time step is small. If a large time step were used, more than one path through the state array might yield an energy balance, thus leading to a lack of uniqueness in the solution. Again since a small time step is needed to model the problem with sufficient accuracy, the explicit finite-difference scheme proved computationally more efficient than more complex schemes.

E. Simulation of nucleation

We now turn to a consideration of the simulation of two- and three-dimensional nucleation events within a one-dimensional calculation. A nucleation event releases latent heat and rapidly raises the temperature of the just-formed seed above that of the surrounding undercooled liquid; for convenience let us assume that this temperature is T_c, the equilibrium melting temperature of the crystalline material. If the undercooling is great, large temperature gradients will be set up and the flow of heat from the growing nuclei may be very rapid, depending on the thermal conductivity of the liquid. If many nucleation events occur in close proximity to one another and more or less simultaneously, the temperature of an extended region will be raised nearly uniformly. The material in this region will be a mixture of solid and liquid that changes as the heat is conducted away and solidification finally occurs.

Now assume that a planar phase interface separating an undercooled liquid such as l-Si and a solid such as a-Si is present in the sample. From Fig. 4 it can be seen that the thermal conductivity of l-Si is an order of magnitude or more greater than that of a-Si. When a nucleation event occurs at or near this interface, the heat liberated will flow rapidly into the liquid and much less rapidly into the solid. Again, if the density of nucleation events occurring nearly simultaneously is high, the temperature of the l-Si will be raised more or less uniformly and the planar interface approximately preserved even though evidence of three-dimensional morphologies may be present in the solidified material. We conclude that the density and frequency of nucleation events, the volume to which they are confined, and the relative magnitude of the liquid and solid thermal conductivities will be important in determining the adequacy of a one-dimensional calculation. Unfortunately, it is unlikely that reliable information about nucleation processes in a given situation will be available. We must then rely on the agreement between experimental and calculated results to establish the appropriateness of a one-dimensional simulation, *ex post facto*.

IV. STATE DIAGRAMS AND ARRAYS

The general assumptions of the modeling, the boundary conditions, and the discretization scheme have been discussed, and we now turn to the two most important innovations of our approach. In order to cope with the variety and complexities of the problems we want to address, it is necessary to have a scheme in which the material in each finite-difference cell can change its phase or its state in accordance with a set of prescribed conditions, and subject only to the requirement of energy conservation. In order to accomplish this, we have introduced the state diagram and the state array which are discussed in this section, together with the interpretation of the mixed two-phase state.

A. The state diagram

Figure 5 gives a form of the state diagram for silicon, while Fig. 6 shows a schematic of the region in the neighborhood of the liquid-solid transitions on an expanded scale. The state diagram is drawn in a manner that reflects our emphasis on enthalpy as the most useful thermodynamic quantity. A horizontal line on the state diagram corresponds to the evolution of latent heat at constant temperature, and therefore to a first-order phase change. There is good evidence that a-Si, unlike true glasses, undergoes a first-order phase change on melting and solidifying. Let us consider examples of successions of changes and transformations that may occur in a small volume of material subjected to heating and cooling.

In the first example, the material is assumed to be initially c-Si and to be subjected to slow heating and cooling.

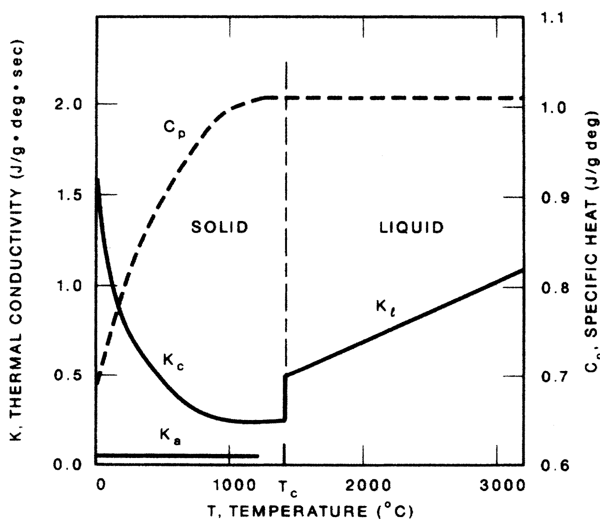

FIG. 4. Thermal conductivity (K) and specific heat (C_p) as a function of temperature for the various phases of silicon. For a-Si, the K_l line is extended toward lower T to T_a at $\sim$1200 °C.

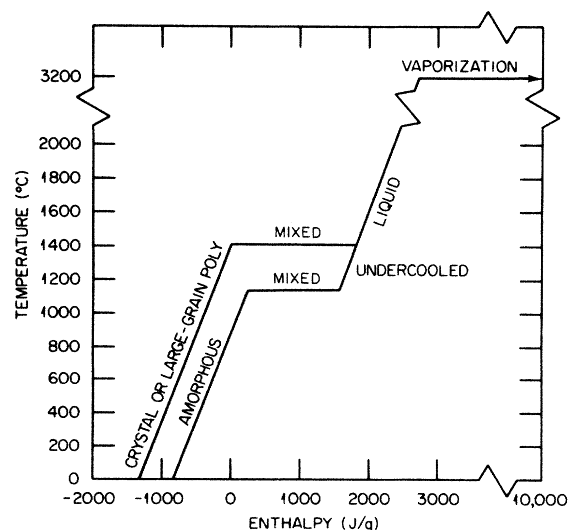

FIG. 5. State diagram for silicon. The zero of enthalpy is taken as that of the crystalline material at the melting point of c-Si.

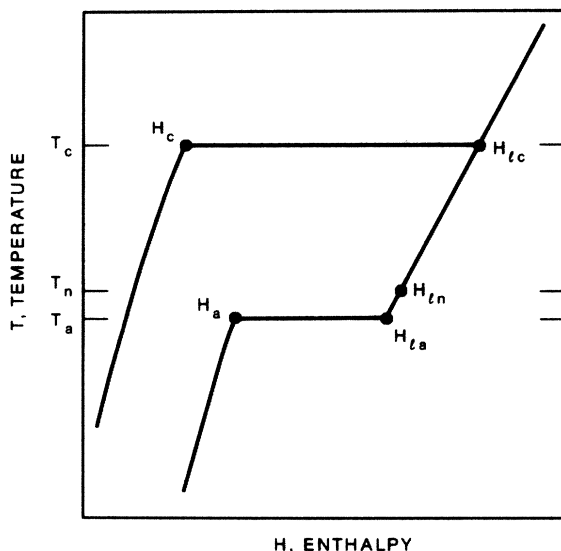

FIG. 6. State diagram for silicon in the neighborhood of the solid-liquid phase transition on an expanded scale.

As the sample is heated, the temperature and enthalpy increase along the line labeled "crystal or large-grain poly" on Fig. 5 until H_c and T_c on Fig. 6 are reached. The material undergoes melting along the line marked "mixed," with the temperature remaining constant at T_c, while the enthalpy changes until enough latent heat is absorbed to completely melt the volume of material under consideration. At H_{lc} on Fig. 6, the temperature of the liquid begins to increase again with increasing enthalpy and continues to do so until the vaporization line is reached. If at some time after melting but before vaporization the material is allowed to cool, the temperature falls until H_{lc} and T_c are reached. When the cooling rate is slow and there is crystalline material contiguous to the material under consideration, there will be little undercooling and the system will very nearly reverse its heating path. This corresponds to near-equilibrium epitaxial growth either from a crystalline substrate or from already-formed crystallites in polycrystalline material. For rapid solidification, undercooling below (H_{lc},T_c) may become nonnegligible even during epitaxial regrowth.

Suppose that the liquid is completely isolated from any solid material that could serve as a template for epitaxial crystallization. Then the liquid may sustain large undercoolings until some nucleation event occurs to initiate crystalline growth or until the system reaches (H_{la},T_a) and amorphous material forms. In fact, it may be possible that such a system could be further undercooled to some state resembling a true glassy material, although this possibility will not be considered here. If no nucleation event occurs, Fig. 6 suggests that the system will return as a-Si. To our knowledge, a-Si has never been formed by slow cooling from the liquid state but the possibility cannot be ruled out. The more common observation is that polycrystalline Si is formed, triggered presumably by a nucleation event in the bulk or at an interface.

Returning now to the state diagram, we consider the difficult question of how to deal with a nucleation event. In the present modeling, as mentioned above, we have assumed that when nucleation occurs, the temperature of the solid seed is suddenly raised to T_c because of the release of latent heat. Although this may seem like a reasonable assumption, it is probably an oversimplification since the kinetics of the nucleation and growth processes and the thermal conductivity will govern the release of latent heat and its rate of diffusion into the surrounding liquid. In other words, the growth of a seed will probably be interface limited. In any case, it is assumed here that a nucleation event in a given cell raises the temperature of the entire cell to T_c by a vertical transition from the H_{la}-H_{ln} line to the H_c-H_{lc} line; such a transition assures conservation of energy. T_n on Fig. 6 is the nucleation temperature and H_{ln} is the corresponding enthalpy; they are utilized in the modeling as follows. If the system (i.e., in practice a finite-difference cell) is undercooled to temperatures in the range from T_a to T_n and remains there for a time t_n, a nucleation event is allowed to occur, provided any additional conditions for nucleation specified by the state array are satisfied.

Our second example of the use of the state diagram deals with the situation shown in Fig. 1, i.e., melting and resolidification of an a-Si layer on a c-Si substrate. In this case the enthalpy and temperature increase along the "amorphous" line of Fig. 5 until (H_a,T_a) on Fig. 6 is reached. The a-Si then begins to melt along the line H_a-H_{la} with the temperature remaining constant. At H_{la} the material is fully molten but highly undercooled. If the temperature remains between T_a and T_n long enough for nucleation to occur, transitions to the H_c-H_{lc} line will be made, as described in the preceding example. If the line segment H_{la}-H_{ln} is traversed rapidly enough, nucleation may be suppressed although the liquid may still be undercooled. For sufficiently high energy input from the laser and/or because of the release of latent heat, the liquid will be heated to $T > T_c$. On cooling, a variety of events, such as those already discussed, can occur depending on the conditions specified in the state array.

Our final example deals with the case in which solidification is so rapid that material that was crystalline before melting is found to be amorphous on solidifying. For simplicity, we assume that the melting part of the process follows the same path as that for the first example considered. On cooling, however, it is required that when the velocity of the melt front reaches some critical value v_a, the liquid does not have time to form a crystalline solid and instead makes a transition to the amorphous phase. Since such high velocities imply large undercoolings, it is again necessary to treat the undercooling in some detail. Moreover, it is apparent that both the magnitude and the *rate* of undercooling are important because, as already noted, a-Si is not formed by slow cooling of l-Si. For example, adhering strictly to the diagram on Fig. 6, it would appear that the material must traverse the line H_{ln}-H_{la} in a time less than t_n so that nucleation can be suppressed, if a-Si is to be formed.

B. Transition states and extended mixed zones

From the standpoint of a finite-difference calculation, any particular cell is said to be undergoing a transition

when the material in the cell is changing from one state to another. The liquid (or solid) fraction in a cell will be determined by the amount of latent heat given up at any time relative to the total amount of latent heat involved in the phase change. More specifically, the transition ratio can be defined as the ratio of heat which has been absorbed or liberated after the transition temperature has been reached to the total heat needed to complete the phase change for the material in the cell. The transition ratio does not locate the phase front within a cell unless additional assumptions are made. If several contiguous cells are undergoing transitions at the same time, the position of a phase front cannot even be defined on the spatial scale of the finite-difference calculation. The material in this extended zone can then be described as in a mixed state, sometimes referred to as "slush." Although this terminology is not elegant, it is descriptive and it is encountered in the literature[33] in various contexts related to the one discussed here (e.g., the growth of dendrities into undercooled liquids).

In those cases where there is a well-defined phase front with an interfacial region much thinner than the finite-difference cell in which it is located, it is clear that reference to the whole cell as consisting of a two-phase mixed state is an outgrowth of the finite-difference formulation. In those cases in which many cells are undergoing transitions more or less simultaneously (as in uniform heating), an extended zone consisting of a two-phase mixed state resembling ice-water slush exists, as described above. An unlikely alternative interpretation would be that the entire extended zone constitutes an interfacial region in which the properties of the material are changing from those of one phase to those of another uniformly. In any case, we believe it is appropriate, and it is certainly useful, to classify the mixed state as a distinct state on the state diagram.

We point out in connection with this discussion that homogeneous or heterogeneous bulk nucleation over regions of only a few finite-difference cells should also lead to the formation of mixed zones consisting of the nucleated solid material embedded in the undercooled liquid.

C. State arrays

Our approach has the capability of treating many different coexisting phases and states. In fact, the only fundamental requirement for a given finite-difference cell is that at any instant its state must be specified by the equation of state, or in other words, its temperature and enthalpy must correspond to a point on the curves of the state diagram. The time evolution of the state of a cell is determined by transitions between points on these curves. We have found it most useful to specify the conditions under which a transition can be made from one state to another in the form of a state array. This array is used to systematize the setting up of a problem and for bookkeeping and is not involved in any algebraic manipulations; its implementation in the LASER8 computer program is by way of a computed branching statement.

Figure 7 gives the simplest nontrivial form of a state array. It would be appropriate for the case in which only

	c	mc	ℓ
c		$H>H_c$	
mc	$H<H_c$		$H>H_{\ell c}$
ℓ		$H>H_{\ell c}$	

FIG. 7. State array for a simple case of melting and crystallization. *c*, crystalline; *mc*, mixed-phase crystalline; *l*, liquid.

melting and crystallization of a single material, e.g., *c*-Si, is considered and overheating and undercooling effects can be neglected. This is the Stefan problem treated so often in the literature and already referred to above (see Refs. 21 and 22). Let us consider how the material in a given cell is transformed from one state to another. The diagonal elements of the array are blank because they represent no change of state. The (c,l) and (l,c) elements are blank because all transitions between solid and liquid states must go through an intermediate mixed-phase state as the melt front moves through a cell. The melting and subsequent crystallization process is given by the sequence $c \to mc \to l \to mc \to c$. Because of the simplicity of this problem, the conditions making up the array elements depend only on the enthalpy and it is not necessary to specify the state of neighboring cells, values of nucleation timers, etc.

Figure 8 shows a version of the complicated state array used in setting up the computer program for studies of the situation depicted in Fig. 1. This version is used here for illustrative purposes and is not necessarily the one most appropriate for reproducing the experimental results that have been obtained for melting of *a*-Si overlayers. Determination of the proper form of the state array for a complex problem can itself become a research undertaking. It should be noted that the state array contains a state labeled "m. fine grain." We found it useful to explicitly introduce such a state even though its latent heat and transition temperatures were assumed to be the same as those for mixed-phase *c*-Si. In the same way, a mixed-phase LG *p*-Si state could have been introduced but we did not find this useful. We will also consider a few of the elements of Fig. 8 and examples of how a cell can be transformed from one state to another.

The first example is a very simple one involving melting of the crystalline state. When the enthalpy of a given cell is increased to $\geq H_c$ the material makes a transition to a mixed-phase crystalline state, as indicated by the (1,6) element in the state array. If the enthalpy continues to increase until $H > H_{lc}$, the cell makes a transition to the normal liquid state with $T > T_c$; this transition is given by the (6,8) element of the array. If there were no amorphous layer present and overheating and undercooling ef-

	1	2	3	4	5	6	7	8	9	
1						$H>H_c$				crystal
2						$H>H_c$				large grain
3							$H>H_c$			fine grain
4					$H>H_a$					amorphous
5				$H<H_a$					$H>H_{\ell a}$	m. amorphous
6	$H<H_c$ 16x x61	$H<H_c$						$H>H_{\ell c}$		m. crystal
7			$H<H_c$					$H>H_{\ell c}$		m. fine grain
8						$H<H_{\ell c}$ s8x x8s			$H<H_{\ell c}$	liquid
9					$H<H_{\ell a}$	$t_1>t_d$	$H<H_{\ell n}$ $t_2>t_n$	$H>H_{\ell c}$		supercooled

FIG. 8. One version of the state array for the melting and resolidification of an a-Si layer on a c-Si substrate. The labels on the right-hand side provide the correspondence with the numbering scheme of the array elements; m. stands for "mixed." t_i and t_2 represent timers contained in the computer program. See the text for further details of the notation.

fects were negligible, melting and subsequent solidification on cooling would follow the sequence $1\rightarrow6\rightarrow8\rightarrow6\rightarrow1$. The (8,6) and (6,1) elements of the array give the conditions on the enthalpy for the indicated transitions to occur, but they also show that certain other conditions involving neighboring cells must be satisfied in more general cases.

Let us introduce a notational form to help in specifying these conditions. The general form employed consists of a sequence of three letters abc and means the following: the cell under consideration is the b cell and it can in principle be assigned any state number, the cell immediately to its left is the one nearer the surface and is labeled a, the deeper-lying neighbor of b is the c cell. When a or c can be any state, they are assigned the letter x. If a neighboring cell is solid but the form of the solid is unimportant, a and c are assigned the letter s. If a neighboring cell is liquid but it is unimportant whether the liquid is normal or undercooled, a and c are assigned the letter l. In all other cases, a state index number will indicate the condition of cells a and c.

Now consider the (8,6) element further. The appearance of the notation $s8x$ means that the b cell (the cell under consideration) is in a liquid state, its neighbor to the left is solid, and the state of the neighbor to its right need not be specified. If these conditions are satisfied, the cell can make a transition to mixed-state crystalline material. However, the cell can also make the same transition if the states of a and c are interchanged. In either case, the b cell is now in a mixed-state crystalline state and can make a transition to crystalline (6,1), LG polycrystalline (6,2), or FG polycrystalline (6,3) if the enthalpy drops below H_c. If the enthalpy of the cell increases above H_{lc} due to additional energy input from the laser pulse or from the release of latent heat in other cells (recalascence), the b cell can remelt.

In the second example, we consider the conditions for each of the transitions that a supercooled liquid cell can undergo according to Fig. 8; these conditions are all on row 9 of the array. The (9,5) element requires that the change from supercooled liquid to mixed a-Si occurs when the enthalpy of the cell falls below H_{la}, the minimum enthalpy that a cell can have and still be entirely liquid. The second possible change, given by (9,6), is from supercooled l-Si to mixed c-Si. For this to occur a timer t_1 (the growth timer) must be greater than t_d, a specified growth delay associated with the interface kinetics. The timer keeps track of how long a supercooled cell has a neighboring cell that is either crystal, large-grained polycrystalline, or fine-grained polycrystalline. This state array assumes that nucleation and growth of a crystalline phase cannot occur off an amorphous interface, although the justification of such an assumption has not been clearly established. The third transition (9,7) is from supercooled liquid to mixed-phase FG material. This was assumed to be the path taken when the liquid nucleates. Two conditions must be met. First, the enthalpy must be less than H_n, the enthalpy above which bulk nucleation is improbable, and secondly a timer t_2 (the nucleation timer) must advance to a time greater than t_n, the specified nucleation time. Finally, element (9,8) indicates that supercooled liquid can change to normal liquid. The condition for the change is that the enthalpy of the cell must equal or exceed H_{lc}, the minimum enthalpy for which normal liquid material can exist.

Before leaving this section we note that conditions specified in the state array can often be obtained from some functional form. For example, the growth timer t_1 could be controlled by an equation such as Eq. (3) and the nucleation timer t_2 by an equation such as Eq. (9).

V. CALCULATIONS

Extensive testing of the modeling described above, as implemented in the LASER8 computer program, was carried out and the results are discussed fully in Ref. 2; pre-

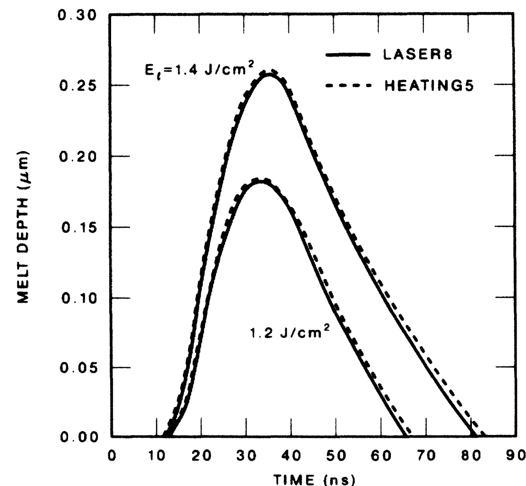

FIG. 9. Comparison of melt-front profiles obtained from LASER8 and HEATING5 calculations for energy densities of 1.2 and 1.4 J/cm^2.

liminary applications of the modeling to the situation shown in Fig. 1 have also been reported.[34] Here we will first demonstrate that for a simple problem LASER8 gives the same results as the more conventional heat-flow calculations and then illustrate some of the additional power of our approach.

In the testing of LASER8, a calculation was run with a triangular (isoceles) pulse of 20 nsec full width at half maximum (FWHM) using temperature-dependent values of the thermal conductivity of Si but a constant value of the specific heat ($C_p = 1$ J/g deg). These choices were made in order to reduce the differences introduced by the use of analytical (LASER8) and numerical (HEATING5) functions for C_p and the pulse shape. Figure 9 compares the position of the melt front as a function of time obtained with the two programs at energy densities of 1.2 and 1.4 J/cm^2. The agreement is very good with the greatest differences being less than the finite-difference cell size of 100 Å. Correspondingly good agreement was also obtained for the surface temperature as a function of time. This example utilized the simple state array of Fig. 7 and the type of curves appearing on Fig. 9 are a familiar way[5] of displaying some of the most important results of the calculations. Note that the derivative at any point on one of the curves of Fig. 9 gives the melt-front velocity.

A. An *a*-Si overlayer on a *c*-Si substrate

The basic problem considered here corresponds exactly to that shown in Fig. 1. One version of a state diagram for it is given in Fig. 8 and discussed extensively in Sec.

TIME (ns)

CELL NUMBERS AND STATES

1 10 20 1 10 20 1 10 20

0.2 J/cm^2 0.4 J/cm^2 0.6 J/cm^2

0 - 10 - 20 - 30 - 40 - 50 - 60 - 70 - 80 - 86 -

FIG. 10. Melting and solidification of an *a*-Si layer on a *c*-Si substrate irradiated with excimer laser pulses of 0.2, 0.4, and 0.6 J/cm^2. The state array was set up to simulate bulk nucleation. Each letter except the left-most represents a cell size of 100 Å; the surface cell is 50 Å.

IV C. We will not go into the details of the problem or the choice of input data except to remark that the a-Si layer was 1850 Å thick, the cell size was 100 Å in the bulk and 50 Å at the surface, and the laser pulse corresponded very closely to that shown in Fig. 3. Instead, attention will be focused on the richness of the results that can be obtained, as illustrated in the following discussion which considers how the effects of bulk nucleation and the phenomenon of "explosive crystallization"[35] can be simulated. We emphasize that the examples given here are not intended to closely replicate experimental results; they were chosen simply to illustrate the capabilities of the approach we have developed.

Figures 10–12 give the results of calculations in a format closely resembling one form of the output used in the LASER8 program. The background letters on the figures give the state of each finite-difference cell at the time printed on the left-hand side. The letters have the following correspondence: C, c-Si; A, a-Si; M, mixed-phase c-, a-, or FG p-Si; S, l-Si below T_c (supercooled); L, l-Si at T_c or above; F, fine-grained polycrystalline material; and P, large-grained polycrystalline material. The heavy lines on the figures indicating the boundaries between the various regions were of course hand-drawn; they correspond to the melt-front profiles of Fig. 9, but are more complicated. The computer program supplies a wide range of information such as the temperature and enthalpy of each cell at any given time, but the format of Figs. 10–12 provides a very graphical picture of the time evolution of the state of each cell.

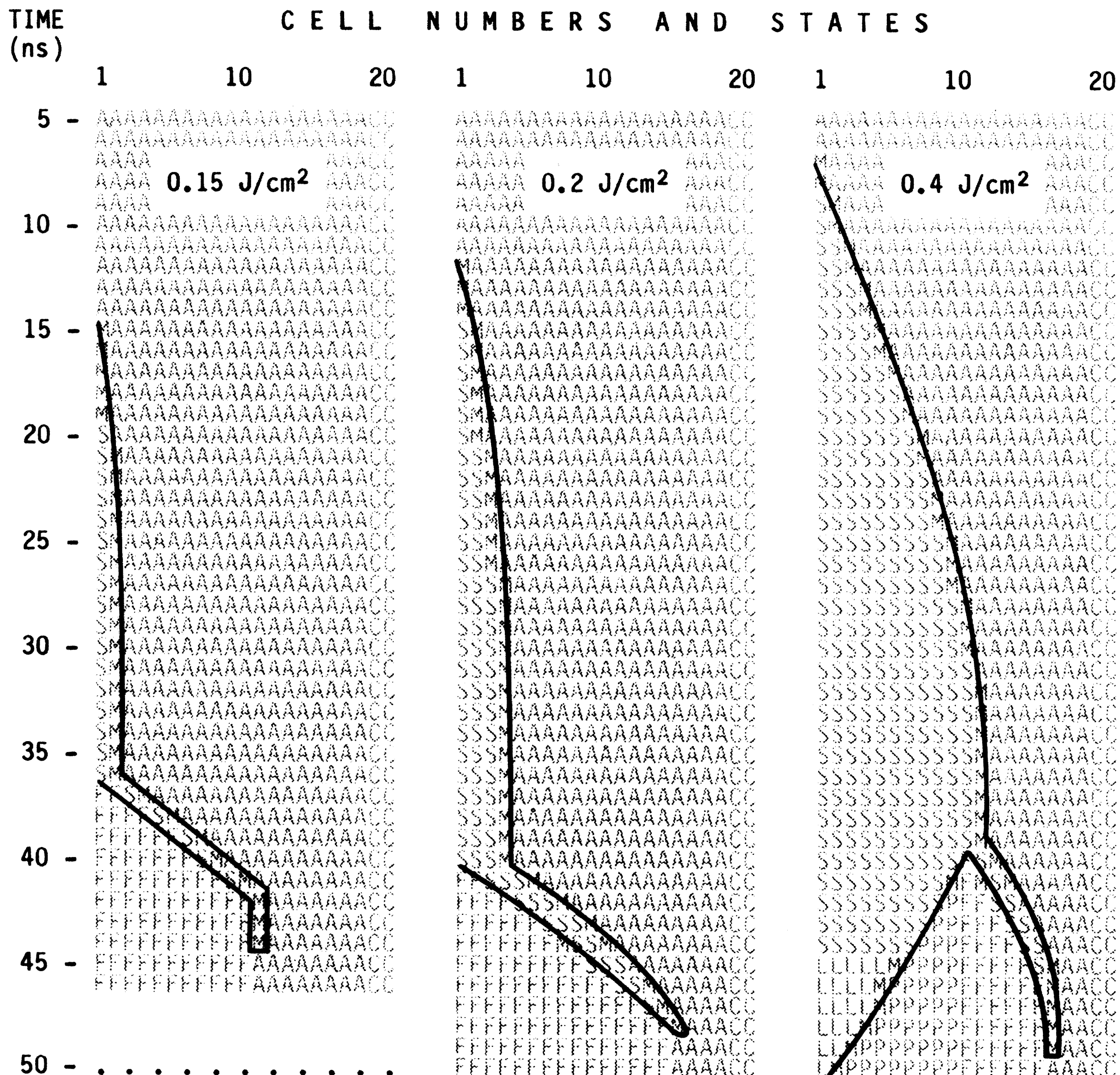

FIG. 11. Results of a calculation similar to that of Fig. 10 but with the computer program modified to simulate "explosive crystallization." The energy densities are given on the figure.

1. Bulk nucleation

Figure 10 shows for three laser energy densities the type of behavior that follows from a simulation in which bulk nucleation, leading to the formation of FG *p-Si*, was forced to play a prominent role. For $E_l = 0.2$ J/cm^2, we see that the material in the first finite-difference cell began to melt at ~ 18 nsec and so became mixed-phase (M) amorphous. The nucleation timer was set at 4 nsec and the nucleation temperature at 1250 °C for these calculations. Since the temperature of the first cell did not exceed 1250 °C within 4 nsec after melting it nucleated at 22 nsec, followed by nucleation of the second cell at 26 nsec. The third cell did not nucleate because the release of latent heat in the first two cells raised its temperature above 1250 °C before it had been molten for 4 nsec. During the time from 20 to 38 nsec, the region from the surface to the melt front consisted of a mixture of solid and supercooled liquid due to bulk nucleation events. The penetration of the melt front into the a-Si was produced primarily by the release of latent heat. This effect becomes particularly apparent after 36 nsec when the surface region had solidified but a buried molten layer continued to penetrate into the solid, driven by the release of the latent heat of crystallization ($L_c = 1800$ J/g) which is greater than the latent heat of melting of a-Si ($L_a = 1319$ J/g). This effect is very similar to explosive crystallization described below but differs from it in that the latent

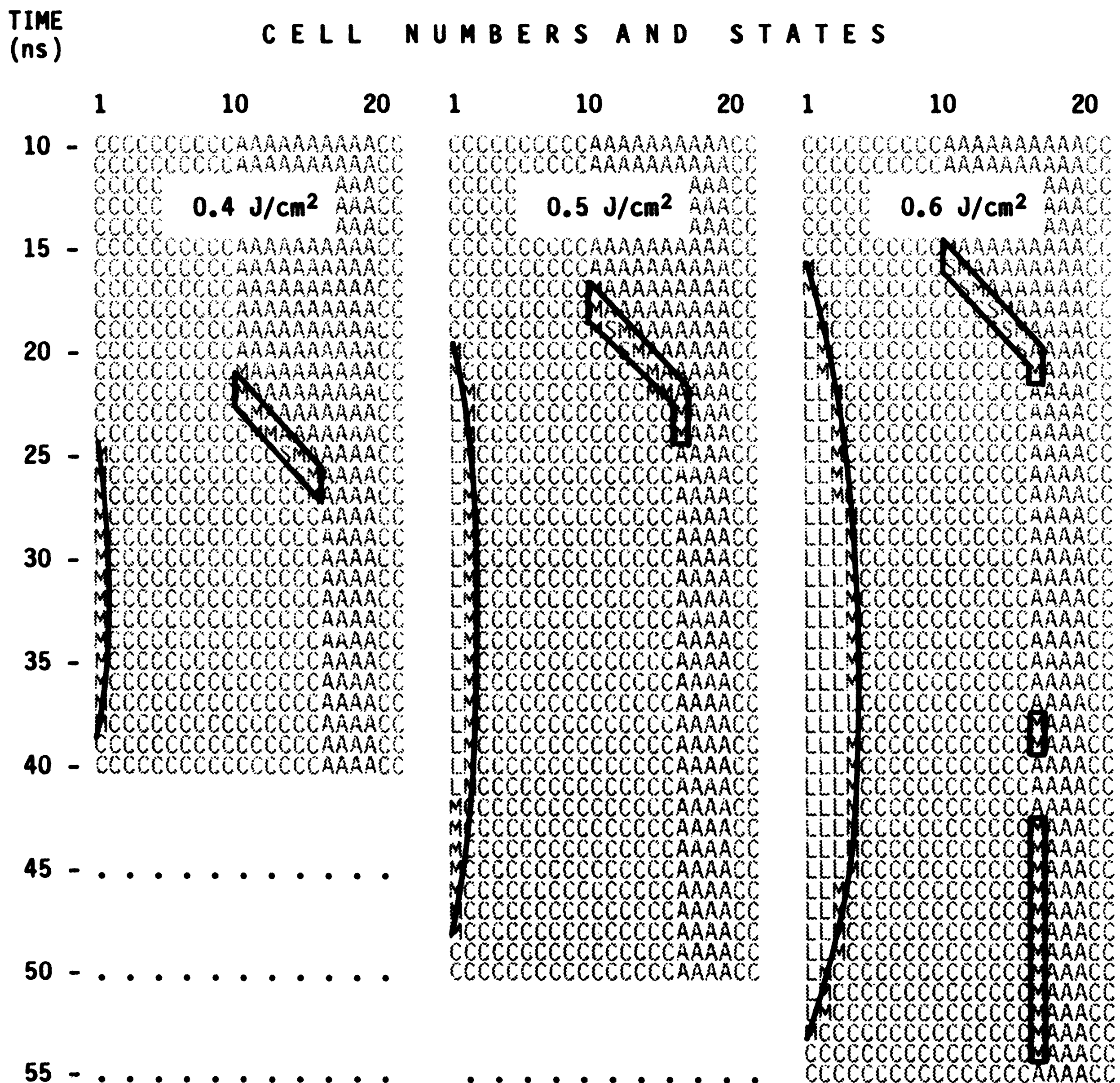

FIG. 12. Results of calculations for an a-Si layer embedded in c-Si and irradiated at three different values of E_l. The state diagram was the same as that used in obtaining the results of Fig. 11.

heat is released by successive nucleation events rather than by growth from a solid-liquid interface trailing behind the melt front (see Fig. 11). The resolidified layer is shown as being composed of a mixture of FG and LG p-Si, however, the LG material with ~ 200 Å grain size would be indistinguishable experimentally from the FG material with ~ 100 Å grain size.

For a laser pulse energy of 0.4 J/cm^2, the first cell began to melt at ~ 10 nsec and 4 nsec later nucleation occurred in it; by the time the first cell nucleated the melt front had penetrated to the fifth cell (~ 500 Å). By the 30th nsec, additional nucleation events and the formation of FG material have occurred in the 3rd, 8th, and 11th cells, resulting in an extended region filled with a mixture of phases and states. At the 38th nsec the maximum melt-front penetration was reached, most of the mixed region had solidified, while the temperature of the molten material near the surface had risen above 1410 °C, as indicated by an L, in the near-surface cells. Finally, at ~ 60 nsec, the melt front originating within this near-surface region returned to the surface and solidification was completed. The appearance of a LG p-Si region within approximately ten cells of the surface and a FG region in the 11th to 15th cells in the solidified material was dictated by conditions specified in the state array, which were chosen to qualitatively simulate experimental observations.

The results for $E_l = 0.6$ J/cm^2 indicate that nucleation occurs only at the surface and near the liquid-solid interface. This behavior results from the fact that although for times less than 30 nsec the majority of the liquid is undercooled for longer than 4 nsec, bulk nucleation does not occur in most cells because the temperature is above the nucleation temperature. Only when the melt front slows down and pauses at its deepest penetration is the liquid below T_n for the 4 nsec required for nucleation. For times greater than 32 nsec, the temperatures of all molten cells, including that of the remelted first two cells, are above the melting point of c-Si at $T_c = 1410$ °C. A well-defined melt front subsequently returns to the surface at a velocity of ~ 4 m/sec.

2. *Explosive crystallization*

Figure 11 shows the results of calculations designed to simulate a somewhat different physical phenomenon than that of Fig. 10. Whereas the modeling leading to the latter allowed bulk nucleation to occur throughout an extended region, the calculations discussed here confined the nucleation events (indicated by the first appearance of FG material) to a region very near, or at the interface. Once a nucleation event occurred, however, the newly solidified material was allowed to serve as a seed for further growth, thus making additional nucleation events unnecessary.

The first panel on the figure shows what might be described as a pure explosive crystallization process. The laser pulse with $E_l = 0.15$ J/cm^2 caused the surface to melt at 15 nsec and the melt front initially just barely penetrated beyond the first cell. The computer program had been modified slightly to require that the nucleation of FG polycrystalline silicon be suppressed until after the melt front had just begun to return to the surface (by monitoring the sign of the melt-front velocity). The release of latent heat from the nucleated cell then drove the melt front into the next cell in a manner similar to that shown for $E_l = 0.15$ J/cm^2 on Fig. 10. However, in the present case, polycrystalline material was allowed to grow off the already crystallized layer at the surface, so that after each new cell was melted it could resolidify by using the material in the cell adjacent to it on the surface side as a seed.

The second and third panels show the evolution of the solidification behavior as the energy density is first increased to 0.2 J/cm^2 and then to 0.4 J/cm^2. This behavior can be described as a mixture of normal and explosive crystallization, with the results for $E_l = 0.4$ J/cm^2 showing the simultaneous propagation of a buried molten layer into the solid and a more normal return of the melt front to the surface from the initially nucleated cell.

B. A buried a-Si layer

A straightforward modification of the situation in the foregoing subsection is to place the a-Si layer beneath a c-Si surface layer. Such an arrangement can be approximated by ion implantation under certain conditions or by a second laser pulse on a sample that initially had the a-Si at the surface and was irradiated with a first pulse that recrystallized a fraction of the a-Si thickness, as in Fig. 11. The calculations for such a situation do not require any modification of the state array used for the explosive crystallization case just considered.

Figure 12 shows the results for a 0.10-μm-thick a-Si layer buried beneath a 0.095-μm-thick c-Si surface layer. At 0.4 J/cm^2, the buried a-Si layer begins to melt at ~ 21 nsec, well before the c-Si surface layer at 25 nsec and "explosively" propagates for ~ 600 Å. In fact, for 0.3 J/cm^2 the a-Si melts without any melting of the c-Si surface layer. Since a purely c-Si sample melts at $E_l \simeq 0.7$ J/cm^2 for the same laser pulse used in these calculations, it is apparent that the low thermal conductivity of the a-Si layer and the release of latent heat on crystallization of the a-Si contribute to the reduction in the pulse energy required for melting of c-Si to a given depth. As E_l is increased first to 0.5 and then to 0.6 J/cm^2, the duration of surface melting increases significantly while the penetration of the buried molten layer into the a-Si increases more slowly. As the a-Si layer becomes thin, it no longer serves as an effective barrier against heat conductance and neither the laser energy nor the latent heat of crystallization are used as effectively in melting the a-Si.

The thin layer of mixed-state material at the c-a interface at longer times may be an artifact of the finite-difference calculation, but the computer output does indicate that this interface stays just at $T_a = 1210$ °C, or very slightly above, for a long period of time. A balance between heat input from the laser and heat flow away from the interface may very nearly hold during this time.

VI. CONCLUDING REMARKS

We have described the conceptual basis, the development, and the implementation of a highly flexible model

for treating laser-induced complex melting and solidification phenomena. At this time LASER8, the computer program based on the modeling, is primarily a research tool, designed to have the capability of addressing some of the most difficult problems presented by experimental results on pulsed laser processing of semiconductors such as Si, Ge, and GaAs. These problems are associated primarily with ultrarapid melting and solidification, and solutions to them must include the role of undercooling and overheating in a phase change, the way in which interfacial kinetics influence (and are influenced by) the undercooling, and the way in which phase nucleation can be simulated in a heat-flow calculation. Since it is not yet clear how best to include all of these effects simultaneously in a calculation, we expect to continue our studies of them and to further refine the basic approach described here. We also hope to extend the modeling to two- and three-dimensional geometries.

The calculations discussed in Sec. V are intended to demonstrate the power of our approach and, as already emphasized, do not necessarily reflect our current thinking on the problems they represent. For example, the solidification processes and resulting morphologies of a pulsed-laser-irradiated *a*-Si overlayer on a *c*-Si substrate are still being studied intensively and the results shown on Figs. 10 and 11 are meant only to illustrate how the complexity that is observed can be understood within the framework of the modeling. To our knowledge, the case considered in Fig. 12 has not yet been investigated experimentally. The results of more refined studies of these problems, taking into account the full range of available experimental data, will be reported in later publications.

Another comment in this same vein concerns the other problem discussed in Sec. II which stimulated the development of our approach, i.e., the transformation of *c*-Si to *a*-Si by pulsed laser irradiation. The results of test calculations with picosecond laser pulses (discussed in Ref. 2) showed regrowth velocities of ~ 100 m/sec, well above the velocity at which *a*-Si should be formed, had it been allowed to occur in the modeling. The processes involved in this transformation almost certainly involve very strong undercooling of the liquid during the return of the melt front to the surface. Although our modeling provides a framework for including this undercooling, the details of how it is to be incorporated into a calculation have not been discussed; this too is a research problem we hope to report on shortly.

Finally, it should be apparent that the techniques described here are applicable to a much wider class of problems than those of laser annealing of semiconductors; the same techniques can be applied to rapid heating and cooling of metals, insulators, and ceramics. Silicon has been emphasized in this paper because it was the material entering most prominently in the development of laser annealing. As we have seen, *a*-Si has a latent heat associated with its melting and solidification that is almost as great as that of *c*-Si (Fig. 5). True glassy materials do not melt or solidify in this way. Because of the great flexibility provided by the state diagram and the state array in combination with a finite-difference formulation, the approach presented here should provide a powerful tool for the study of the glass transformation in glass-forming materials.

ACKNOWLEDGMENTS

We would like to thank V. Alexiades, J. B. Drake, G. E. Giles, G. E. Jellison, Jr., D. H. Lowndes, A. D. Solomon, and F. W. Young, Jr. for many useful discussions bearing on topics covered in this paper.

---

[1]Several general references on this subject are *Pulsed Laser Processing of Semiconductors,* Vol. 23 of the *Semiconductors and Semimetals* series, edited by R. F. Wood, C. W. White, and R. T. Young (Academic, New York, 1984); *Laser Annealing of Semiconductors,* edited by J. M. Poate and J. W. Mayer (Academic, New York, 1982); and the volumes in the series of Proceedings of the Materials Research Society, published by North-Holland.

[2]G. A. Geist and R. F. Wood, Oak Ridge National Laboratory No. ORNL-6242, 1985 (unpublished); available from the authors or from National Technical Information Service, U. S. Department of Commerce.

[3]HEATING5 is a recent version of a computer program HEATING that was originally developed by several groups of workers; HEATING is an acronym for heat engineering and transfer in nine geometries. HEATING5 is described at length in Ref. 4.

[4]W. D. Truner, D. C. Elrod, and I. I. Siman-Tov, Oak Ridge National Laboratory Report No. ORNL/CSD/TM-15, 1977 (unpublished). Available from National Technical Information Service, U. S. Department of Commerce.

[5]R. F. Wood and G. E. Giles, Phys. Rev. B **23**, 2923. This paper describes some of the modifications made to HEATING5 to adapt it to calculations of the effects of pulsed laser irradiation of semiconductors. See also Chap. 4 of the first volume in Ref. 1.

[6]Semiconductor processing with cw lasers is also of general interest, but since melting seldom occurs in applications involving cw lasers we restrict our attention to pulsed lasers.

[7]R. Tsu, R. T. Hodgson, T. Y. Tan, and J. E. Baglin, Phys. Rev. Lett. **42**, 1356 (1979).

[8]P. L. Liu, R. Yen, N. Bloembergen, and R. T. Hodgson, Appl. Phys. Lett. **34**, 864 (1979).

[9]A. G. Cullis, H. C. Weber, N. G. Chew, J. M. Poate, and P. Baeri, Phys. Rev. Lett. **49**, 219 (1982).

[10]See, for example, E. P. Donovan, F. Spaepen, D. Turnbull, J. M. Poate, and D. C. Jacobson, Appl. Phys. Lett. **42**, 698 (1983), and references therein.

[11]A. G. Cullis, Mater. Res. Soc. Symp. Proc. **13**, 75 (1983).

[12]H. C. Webber, A. G. Cullis, and N. G. Chew, Appl. Phys. Lett. **43**, 669 (1983).

[13]D. H. Lowndes, R. F. Wood, and J. Narayan, Phys. Rev. Lett. **52**, 561 (1984).

[14]M. O. Thompson, G. J. Galvin, J. W. Mayer, P. S. Peercy, J. M. Poate, D. C. Jacobson, A. G. Cullis, and N. G. Chew, Phys. Rev. Lett. **52**, 2360 (1984).
[15]J. Narayan and C. W. White, Appl. Phys. Lett. **44**, 35 (1984).
[16]R. F. Wood, D. H. Lowndes, and J. Narayan, Appl. Phys. Lett. **44**, 770 (1984).
[17]Indications of such features are found in Ref. 15, and they are prominent in recent data of D. H. Lowndes and co-workers (unpublished).
[18]K. A. Jackson and B. Chalmers, Can. J. Phys. **34**, 473 (1956).
[19]D. Turnbull, Solid State Phys. **3**, 225 (1956).
[20]See Chap. 5 of the first volume of Ref. 1 and references therein.
[21]See, for example, H. S. Carslaw and J. C. Jaeger, *Conduction of Heat in Solids,* 2nd ed. (Clarendon, Oxford, 1959), p. 282.
[22]J. R. Cannon, in *Moving Boundary Problems,* edited by D. G. Wilson, A. D. Solomon, and P. T. Boggs (Academic, New York, 1978), p. 3.
[23]Virtually all rigorous treatments of heat flow and phase change during pulsed laser irradiation of materials have been carried out within the framework of the Stefan problem.
[24]J. H. Holloman and D. Turnbull, Prog. Metal. Phys. **IV**, 333 (1953); J. W. Cahn and J. E. Hilliard, J. Chem. Phys. **28**, 258 (1958); **31**, 688 (1959); J. S. Langer, Ann. Phys. (N.Y.) **54**, 258 (1969); P. Harrowell and D. W. Oxtoby, J. Chem. Phys. **80**, 1639 (1984).
[25]M. Grant and J. D. Gunton, Phys. Rev. B **32**, 7299 (1985).
[26]C. S. Hsu and A. Rahman, J. Chem. Phys. **70**, 5234 (1979); R. D. Mountain and P. K. Basu, *ibid.* **78**, 7318 (1983).
[27]V. Alexiades, J. B. Drake, G. A. Geist, G. E. Giles, A. D. Solomon, and R. F. Wood, Oak Ridge National Laboratory Report No. ORNL-6129 (unpublished); available from National Technical Information Service, U. S. Department of Commerce.
[28]J. Crank, *Numerical Methods in Heat Transfer,* edited by R. W. Lewis, K. Morgan, and D. C. Zienkiewicz (Wiley, New York, 1981).
[29]M. Rose, Math. Comput. **14**, 249 (1960).
[30]See A. Solomon, Math. Comput. **20**, 347 (1966), for further elaboration of the method.
[31]M. von Allmen, Mater. Res. Soc. Symp. Proc. **13**, 691 (1983), has applied an enthalpy equation to laser quenching problems.
[32]See the discussion and references in Chaps. 4 and 6 of the first volume of Ref. 1.
[33]Examples of such terminology are contained in A. D. Solomon, D. G. Wilson, and V. Alexiades, Lett. Heat Mass Transfer **9**, 319 (1982), and in references therein.
[34]R. F. Wood, G. A. Geist, A. D. Solomon, D. H. Lowndes, and G. E. Jellison, Jr., Mater. Res. Soc. Symp. Proc. **35**, 159 (1985).
[35]Explosive crystallization is a well-documented phenomenon first observed in *a*-Sb films in the last century [G. Gore, Philos. Mag. **9**, 73 (1855)]. It has played a prominent role in explaining the crystallization of amorphous layers by cw lasers [see, e.g., G. Auvert, *et al.,* Appl. Phys. Lett. **39**, 724 (1981)] and more recently Thompson *et al.* (Ref. 14) proposed it as the basic mechanism for the formation and propagation of buried molten layers during the pulsed laser irradiation of *a*-Si.